COBEM 2023 27TH INTERNATIONAL CONGRESS OF MECHANICAL ENGENEERING

ABCM Brazilian Society of Mechanical Sciences and Engineering
27th ABCM International Congress of Mechanical Engineering
December 04-08, 2023, Florianópolis-SC, Brazil

COBEM-2023-0879
NUMERICAL INVESTIGATION FOR SUPERSONIC GAS SEPARATOR WITH CURVED NOZZLE

Denis Fernando Gregório Júnior, BSc Eng.
Universidade de São Paulo, Escola Politécnica, Departamento de Engenharia Mecânica, Av. Prof. Mello Moraes, 2231, São Paulo, SP, Brazil.
denis.fernando@usp.br

Reinaldo Marcondes Orselli, PhD
Univesidade Federal do ABC, Centro de Engenharia, Modelagem e Ciências Sociais Aplicadas, Avenida dos Estados, 5001, Santo André, SP, Brazil
reiorselli@gmail.com

Ricardo Galdino da Silva, PhD
Instituto de Aeronáutica e Espaço, Departamento de Ciência e Tecnologia Aeroespacial, Praça Marechal Eduardo Gomes, 50, São José dos Campos, SP, Brazil
ri_galdino@yahoo.com.br

Bruno Souza Carmo, PhD
Universidade de São Paulo, Escola Poltécnica, Departamento de Engenharia Mecânica, Av. Prof. Mello Moraes, 2231, São Paulo, SP, Brazil.
bruno.carmo@usp.br

Abstract. *Supersonic gas separators are devices that allow the separation of heavier components of natural gas through supersonic flow expansion through a convergent-divergent nozzle. The temperature decreases along the divergent section until condensation of some components occurs with the formation of liquid droplets. The droplet separation is done by imposing centrifugation which conducts the condensed particles towards collectors attached to the nozzle wall. A key beneficial aspect of such supersonic separator devices is related to their compactness combined with the absence of moving parts, resulting in a small footprint and low maintenance cost. In this context, the purpose of this work is to investigate, through numerical simulations, the flow behavior of a supersonic convergent-divergent nozzle, as used in the supersonic gas separator device, but with a nozzle of curved shape to generate centrifugal force. The Finite Volume Method is used for the numerical simulations. Due to the high turbulence in the flow, the flow is resolved based on RANS (Reynolds Averaged Navier-Stokes) equations, particularly, with the k-ε RNG and k-ω SST turbulence models. Subsequently, the curvature of the initial geometry is modified in order to generate higher centrifugal force; parameters such as the radius of curvature and the length of the supersonic section are reduced. Flow features along the nozzle length such as pressure distribution, temperature, centrifugal force level as well as shock wave topology and position are shown and analyzed. With the different curvature shapes tested, the centrifugal force attained levels ranging from 118000g up to 214000g. Particularly, in comparison with a straight nozzle, due to the curvature shape, a sequence of several slight oblique shock waves was noticed in the supersonic expansion region. A possible explanation for this sequence of oblique shock waves is that along the curved supersonic expansion, the flow path of the inner nozzle arch side is shorter with respect to the outer arch side that has a longer path.*

Keywords: *Computational Fluid Dynamics, Turbulence models, Fluid Mechanics, Shock Wave, Supersonic Separator*

1. INTRODUCTION

Due to the discovery of the oil and gas reserves, the growth of exploration of these resources in offshore regions has increased the demand for technological solutions that facilitate the extraction and refining processes, as well as the commercialization oil and its derivatives directly or close to their extractive regions (Lima, 2016).

Among the fossil fuels, natural gas has shown potential for applicability due to its good energy response to lower CO_2 emissions compared to coal and oil, where the greatest challenges for its use are based on the removal of impurities at the time of extraction (Wen et al., 2012). Water particles, presence of different acids and high concentrations of hydrocarbons, in particular CO_2, are present in raw natural gas as well as in other fuels, where the direct displacement of these to decontamination zones in regions far from the extraction point takes risks of safety and higher costs due to the corrosive effects that the cited heavy components develop. Thus, it is necessary to implement techniques and equipment that allow the purification of natural gas directly from the extraction point or in nearby locations.

The supersonic separator avoids hydrate problems and eliminates the need for inhibitor and regeneration systems due to short fluid residence time in the device, providing an environmentally friendly technology. As a static device, there are no rotating or moving parts so increasing reliability and availability. Therefore, it is suitable for unmanned operations, especially on platforms. Supersonic separation technology is significant for the development of the natural gas industry in a way of safety, environmental protection and energy conservation. In view of the good performance of this technology, many researchers have studied about the design, performance, efficiency, economics, feasibility and industrial applications of supersonic separator (Cao & Bian, 2019). The mechanism consists of a convergent divergent nozzle where the gases are accelerated to supersonic speed and expanded isentropically, generating a drop in temperature. With cooling, some of the contaminants, such as CO_2, are condensed while the hydrocarbons remain in a gaseous state. By imposing rotational flow forces, the heavier condensed components are pushed towards the wall where the collectors are carefully placed to remove them.

The internal flow of supersonic separators presents complex physical behaviors such as the formation of shock waves and consequent interactions with the boundary layer. The increase in entropy and temperature characteristic of normal shock waves directly impact the operation of the equipment. With the results referring to the nozzle simulations with the straight axisymmetric supersonic section already known (Yang et al., 2014); in order to verify the effects of centrifugation in the nozzle, as well as oblique shock waves, an analysis with the curved supersonic section with different radius of curvature and angles is necessary. Due the curved nozzle shape, this type of configuration does not need fins to generate centrifugation as the curvature itself is designed to generate the centrifugal force. With the nozzle curvature associated with centrifugation, the heavier components that have higher density will accumulate along the nozzle elbow, allowing their separation from the main flow, where a collector is installed. Thus, the geometry would not have the conventional axisymmetric circular cross section, instead being a duct with a planar cross section.

An example of the Orbital ATK and ACENT Laboratories can represent the main advantage of using a curved section due to the concentration of unwanted particulates in only one side of the nozzle indicated in Fig 1.

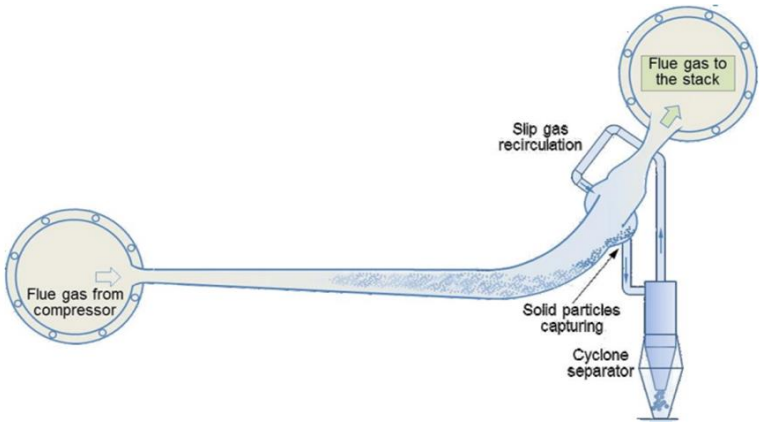

Figure 1. Schematic of ICES process showing the converging-diverging supersonic nozzle for solid CO_2 particle formation, inertial CO_2 capture duct, and pressure recovery in gas diffusor before outlet to the stack (Berger, 2016).

However, the quality and accuracy of numerical simulations to predict the behavior of such gases in supersonic separators are essential to carry out an adequate design developed around good practices. One of the typical problems related to numerical simulation of highly turbulent flows is the ability of the CFD based on turbulence models to properly represent the existing phenomena given an adequate simulation model.

2. OBJECTIVE

The objective of this work is to investigate the influence of the curvature in a convergent divergent nozzle in relation to the effects of centrifugation, and the flow behavior on the nozzle walls through numerical simulations with reference to numerical results with the case of the available straight section as available in the work of (Yang et al., 2014). In particular, the case corresponds to a convergent-divergent supersonic nozzle geometry in (Yang et al., 2014) using air as the working fluid. In the present work, the commercial code ANSYS FLUENT is used for numerical simulations whose solver is based on the Finite Volume Method.

In order to carry out numerical simulations, the computational domain of the flow is considered primarily as planar two-dimensional. Due to the high turbulent flow, different turbulence models are used. The turbulence models considered for this work are the following: k-ε RNG (Yakhot et. al, 1992) and k-ω SST (Menter et. al, 1993).

3. METHODOLOGY

The route used to carry out the numerical simulation consists of constructing the geometry using the ANSYS Workbench itself via SpaceClaim, which is the CAD generator from ANSYS, followed by the use of ANSYS MESHING for the discretization of the geometry domain and ANSYS FLUENT as solver and post-processor code.

In the ANSYS FLUENT code, the Navier-Stokes equations are solved numerically, and the flow domain is discretized by applying the finite volume method (Versteeg & Malalaskera, 2007), in which, one known is the pressure-based solver which uses the segregated method approach to solving state variables. For the present application, the segregated solver was considered with the equation of state incorporated to deal with the highly compressible nature of the flow within the nozzle (see methodology in Maliska, 2004).

To deal with the high turbulent flow and avoid the prohibitive computational cost of solving all turbulent flow scales, the Navier-Stokes equations are averaged with each flow variable decomposed with a time average and a floating part (known as Reynolds decomposition). As a result of the time-averaged Navier-Stokes equations, a nonlinear term dependent on the floating part of the flow velocities remains, which is known as the Reynolds stress tensor. To close the set of equations of the mean Navier-Stokes equations, also known as RANS (Reynolds Averaged Navier-Stokes) equations, additional transport equations are needed due to the Reynolds stress tensor term, as it is dependent on the floating part of the velocities flow. First, the term Reynolds-stress tensor can be related to the mean flow, considering the Boussinesq hypothesis (see Versteeg & Malalaskera, 2007), which in turn introduces a new coefficient known as turbulent viscosity due to its related physical interpretation additional turbulent mixing flow in relation to fluid viscosity. Then, the unknown turbulent viscosity is modeled relating it to new turbulent flow variables. Finally, to close the RANS equations, additional transport equations for these turbulent flow variables are proposed. There are several turbulence models in the literature that propose a relationship for turbulent viscosity with different turbulent flow variables and transport equations (Versteeg & Malalaskera, 2007). The turbulent models considered for this work are k-ε RNG (Yakhot et al, 1992) and k-ω SST (Menter et. al, 1993); all models are available in Ansys Fluent code (Ansys Inc, 2013).

4. RESULTS

4.1 Geometry and Mesh

The geometry of the nozzle used from the numerical work of (Yang et al., 2014) using the method described in (Foelsch, 1945) for the preservation of the isentropic behavior at the beginning of the throat to its divergent section is shown in Fig. 2. Due to the character of the flow presumably having Mach waves, in addition to deflection phenomena on one side of the walls due the curved nozzle, the flow does not have a symmetrical nature. The planar geometry was used and adapted from the design of (Yang et al., 2014 and denoted by figure 4) also increasing by 1.5x the length of the diffuser to the end of the supersonic section, totaling a length of 801 mm instead of the previous 543 mm. The choice of increase is to have the amortization of the gas velocity and pressure fields. The convergent geometry was made by fitting a quadratic polynomial of the nozzle geometry as mentioned in (Yang et al., 2014) preserving the measurements.

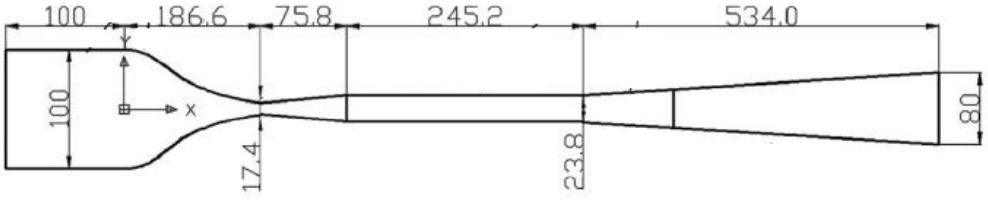

Figure 2. Original nozzle geometry with measurements in millimeters [mm] by (Yang et al., 2014)

Regarding curvature, as a pre-definition for initial studies, we decided to preserve the original length of 245.2 mm of the supersonic section, and, considering the definition of G force:

$$\text{G Force} = \frac{acceleration\ in\ m/s^2}{gravitational\ acceleration} = \frac{a}{9.81} \tag{1}$$

$$\text{a} = \frac{v^2}{r} = v\omega = \omega^2 r \tag{2}$$

Where v = velocity magnitude of nozzle (in m/s); r = radius of curvature of a perfect arc of circumference (in meters), used for the construction of the curve the supersonic nozzle section, denoted in Fig. 5; ω = angular velocity (in rad/s) and 9.81 as the acceleration of gravity (in m/s^2). Due to the fact that the geometry has a curve, the gas acceleration has a

centrifugal component, where the acceleration modulus and the velocity field are larger than the nozzle with the supersonic straight section. Accordion to (Duan et. al 2009 and Wen et. al 2010), the separation is efficient when the G force is between 270000 G and 800000 G. For the execution of the first analyses, 100000 G was the predetermined initial value and the initial supersonic velocity was the maximum velocity magnitude of the straight case.

The planar straight case described in Fig. 3 was simulated with a 44100 cell mesh. The non-dimensional distance from the wall of the first cell adjacent to the wall is known as *y+* (definition in Versteeg & Malalasekera. 2007). The boundary layer has a logarithmic region that is approximated between y+ between 31 and 500 (as described in Versteeg & Malalasekera. 2007).

In this context, a wall model is used taking into consideration this behavior of the logarithmic law, making it possible to set a value of y+ in this region in combination with an appropriate mesh refinement to capture the velocity gradients along the boundary layer (as it is the case here of y+ between 75 and 125). For a preliminary assessment of the effects of changing the geometry, the choice of working fluid will not initially have mixtures, being a single-phase using air as the working fluid, thus, also not considering condensation and evaporation effects, also for particle injection, which can be developed in future stages with working fluids closer to the real behavior. The NPR (Nozzle Pressure Ratio is the ratio of inlet and outlet pressure) was 1.54, with 100000 Pa of inlet pressure and 65000 Pa of outlet pressure.

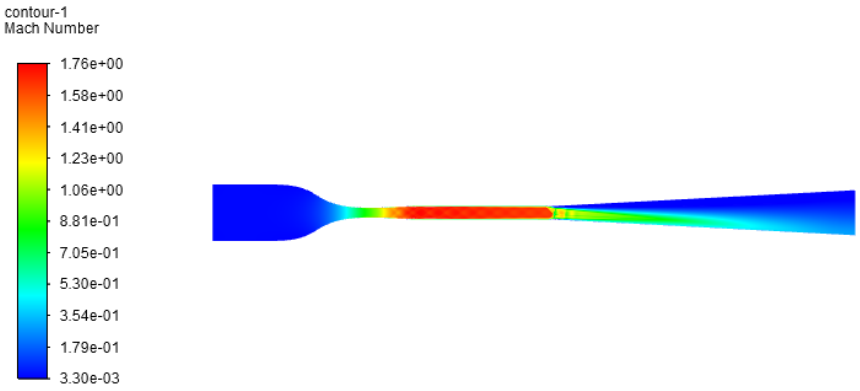

Figure 3. Straight case Mach field

The maximum Mach number of 1.76 (described in the Fig. 3 label) implies in 466 m/s as the maximum velocity magnitude. According to G-force formula (2); the radius of curvature returned a 0.221 m and the angle could be reached by the arc length formula, resulting of 63.42°, as shown in Fig. 4a and 4b. An additional configuration with a gas collector aside the diffuser inlet was considered.

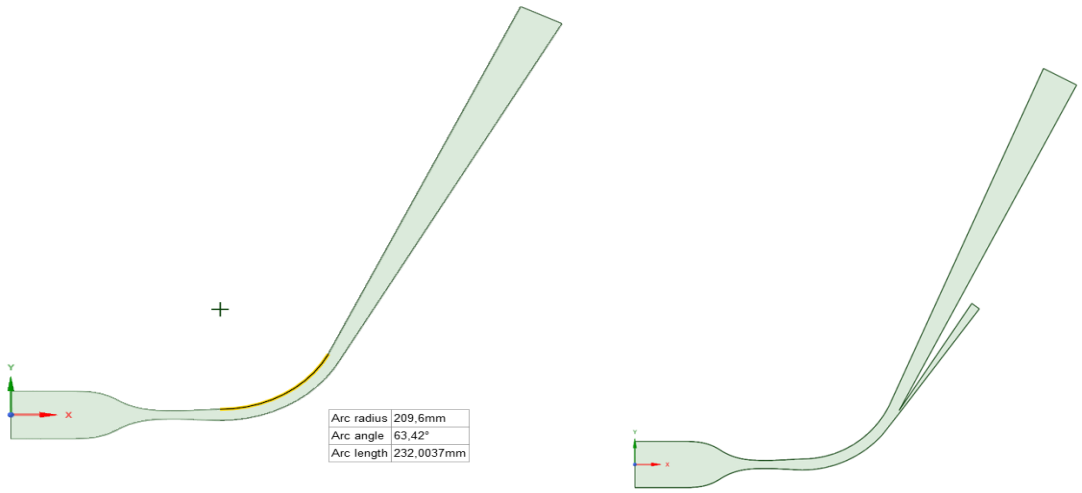

Figures 4a and 4b. Full geometry with original length (left) and with the gas collector (right)

For the nozzle with a two-dimensional domain, as shown in Fig. 4a and 4b, a structured mesh was constructed with a total of 52200 and 86000 cell volumes in the figures 5.1 to 5.3. The dimensionless distance from the wall, defined by *y+* for this mesh configuration was between 25 and 125 in the shock wave region and 10 at other regions.

The method used for construction was to focus the mesh refinements on velocity gradients, that is, in ascending order of cells from when the convergent section starts to the beginning of the supersonic section. A mesh refinement is also carried out where there is a shock wave at the entrance of the diffuser, with the diffuser itself being considerably reduced along its longitudinal direction in order to save computational resources.

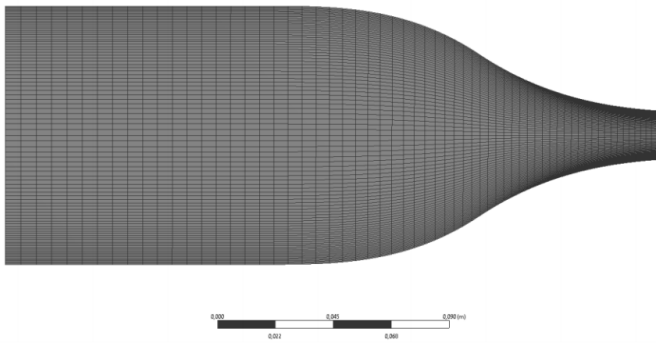

Figure 5.1. The convergent section mesh

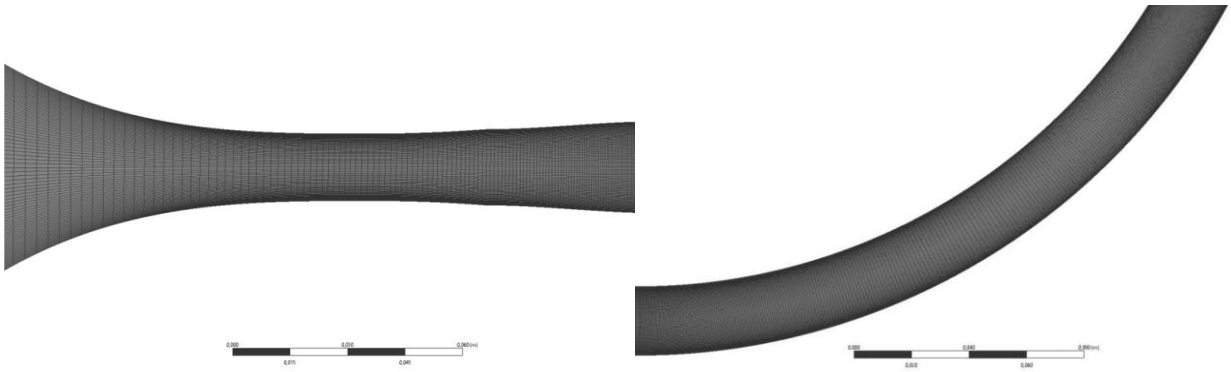

Figures 5.2a and 5.2b. The throat and divergent section mesh (left) and the supersonic section mesh (right)

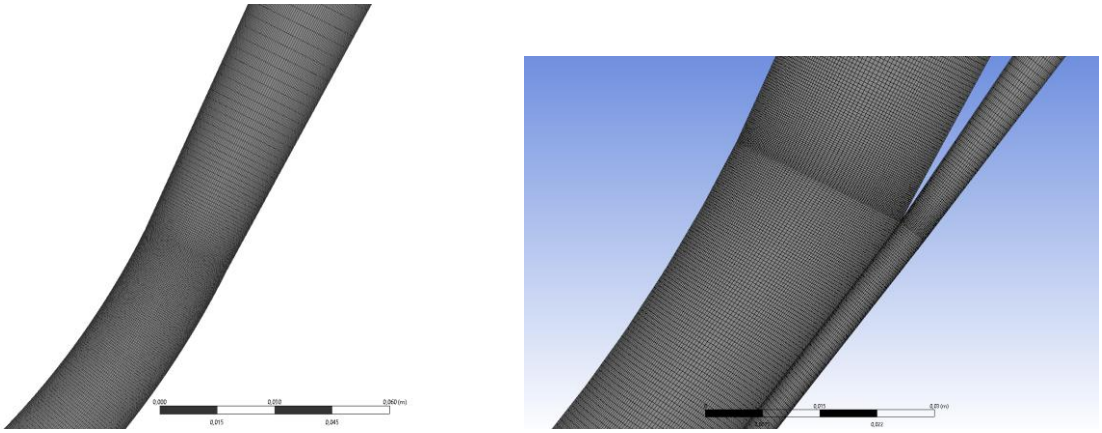

Figure 5.3a and 5.3b. The diffuser section mesh without (left) and with the gas collector (right)

4.2 Numerical Setup

The cases with and without the gas collector was considered first. For the boundary conditions, the total pressure and the total temperature in the inlet section (reservoir condition) and the static pressure and the total temperature fixed in the outlet section were defined, following a NPR of 1.54 for the case without the gas collector, as the straight case, and 2.22 in the case with the gas collector present. For the gas collector, the outlet pressure is the same of the diffuser exit. No-slip adiabatic wall was applied at the upper edge of the nozzle and symmetry condition for the axis line. The fluid was considered a perfect ideal gas and the values used for the boundary conditions are shown in Table 1.

Table 1. Boundary conditions for the simulation

	Static Pressure	**Total Pressure**	**Total Temperature**	**Gas Collector present**
Inlet	100000 Pa	101325 Pa	291 K	-
Outlet	65000 Pa	-	291 K	No
Outlet (diffuser and collector)	45000 Pa	-	291 K	Yes

So, in order to resolve the flow gradients in the wall region and deal with the wide range of y+ values, the log-law region from the law of the wall (with y+ varying between 31 and 500, see in Versteeg & Malalasekera, 2007, pg. 59) was used and is within the degree of accuracy that is described by the wall law by the solver itself, based in y+ ranges bewteen 125 and 200 for the present case. (see Ansys Inc, 2013).

For the two-dimensional simulations, according to the Ansys Fluent pressure-segregated solver, to deal with the pressure-velocity coupling, a scheme known as Coupled (Ansys Inc, 2013) was used. This algorithm allows solving the momentum and continuity equation together, which can bring a better numerical convergence compared to other well-known schemes such as SIMPLE (Versteeg & Malalasekera, 2007). Furthermore, for all simulations a second order upwind scheme was applied to all convective terms of the transport equations (Barth and Jespersen, 1989), and the diffusive terms were discretized by a central difference scheme (Versteeg & Malalasekera, 2007). In order to obtain pressure on the faces of the control volume, an interpolation scheme based on a "staggered" control volume arrangement was employed for all cases (known in ANSYS Fluent as PRESTO, PREssure Staggering Option, Ansys Inc, 2013).

Regarding the numerical convergence criteria of Ansys Inc (2013), as a general reference, at least a maximum residual value of 1e-04 for all transport equations, and a maximum residual value of 1e-6 for the energy transport equation, is recommended. Residuals are defined in Ansys Fluent as the imbalance of each discretized transport equation added to all domain cells in the current iteration scaled by the flow of the main variable in the cell center according to each equation (Ansys Inc, 2013). Table 2 shows the residual values obtained for the k-ε RNG model, all with the same mesh.

Table 2. Residuals results from the simulation

Gas Collector present	**Model**	**Continuity**	**x-velocity**	**y-velocity**	**Energy**	**k**	**ε**
No	k-ε RNG	3,72E-06	5,11E-05	1,79E-05	9,68E-06	1,46E-05	9,63E-04
Yes	k-ε RNG	2,72E-05	1,79E-05	1,34E-05	0,42E-06	0,46E-04	1,63E-05

4.3 Mesh Influence Analysis

Although some approximations have already been made for the number of cells to reach 52200, it was still necessary to carry out an influence analysis to verify how much the mesh refinement influenced the solutions.

At first, the number was multiplied by the root of 2 (73660 cells) and divided by the root of 2 (36540 cells) for the purpose of the test interval, where, in the analysis of final velocities, it did not present greater variations. In relation to the processing time, for the case of 36540 cells, the processing time and total management of the methods was significantly higher due to the initial data being calculated with less precision, requiring high iteration shifts.

The case of 73660 cells has already presented identical results, which indicates that the number of 52200 is a suitable value from a computational point of view for the case without the collector. With the gas collector present, the number of 52200 cells increases to 86000 due the growth of geometry due the introduction of the device, maintaining the same *y+* number in the entire computational domain.

4.4 Two-dimensinal Results

The first tests were carried out to verify the simulation before the mesh verification steps. Using 52200 and 86000 cells in the mesh, the static pressure, the Mach number field and variation along the nozzle length and the G force distribution (respectively figures 6, 7, 8 and 9) are plotted as:

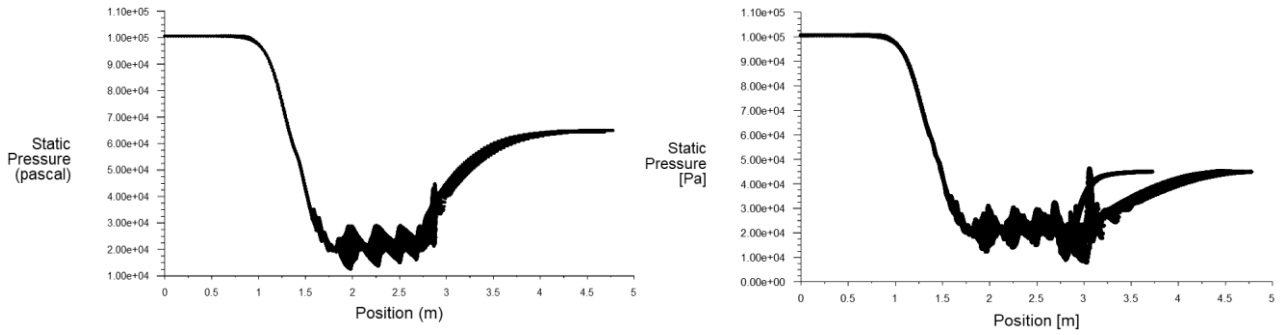

Figures 6a. and 6b. Static Pressure distribution against the nozzle length (in the x direction) for the case without the gas collector (Fig. 4a., left) and with the gas collector (Fig. 4b., right).

The graphs in the Fig. 6a. and 6b. show the pressure distribution of the whole inner part of the nozzle and along the entire transverse direction. There is the presence of multiple curves along the flow, going from upstream to downstream of the nozzle, one for each cell in the cross section, including the aggregate collector. The set of curves denotes the presence of multiples obliques shock reflections as well as variation of pressure values in the supersonic section. The curves depicted on the static pressure graph indicate the maximum and minimum pressure range along the curve and at the diffuser inlet. In Fig. 6b, it is verifiable that there are two static pressure outlets due to the presence of the collector near 3 meters.

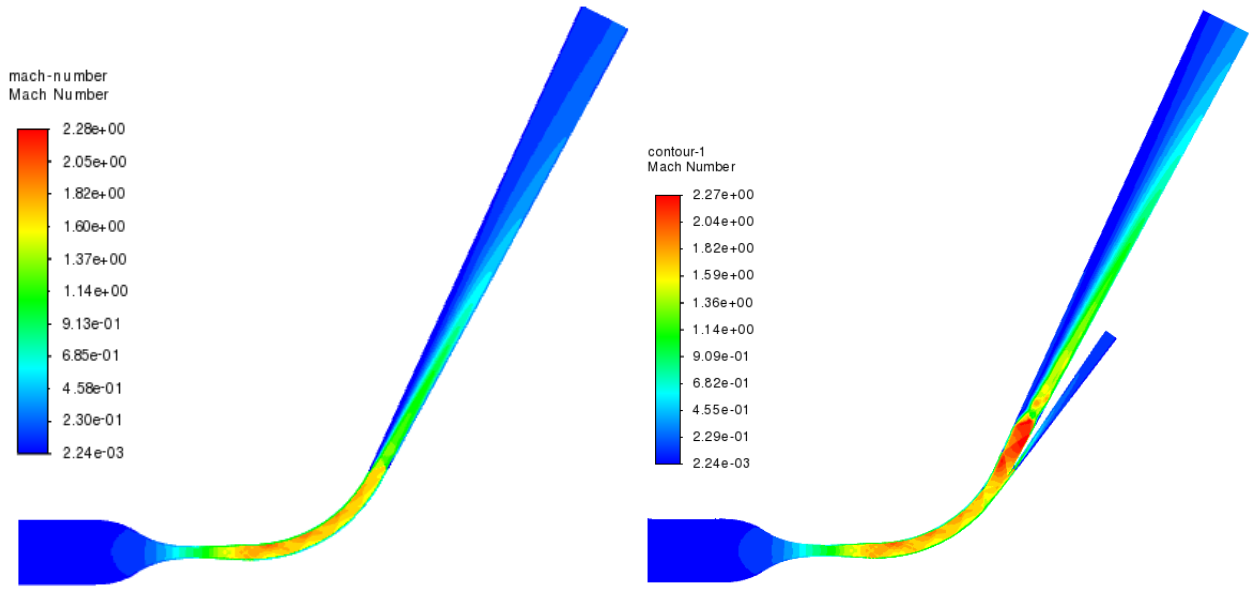

Figures 7a and 7b. Mach contours field for the case without the gas collector (left) and with the gas collector (right).

In Fig 7a. and 7b., oblique weaker shocks are observed that are reflected along the supersonic section with a pressure variation of approximately 6 kPa in the supersonic region. At the end of the curved section and beginning of the diffuser a strong shock is observed, and then downstream the flow becomes subsonic where there is a pressure recovery until the diffuser outlet. In the diffuser, an asymmetry is observed, due to the separation of the flow due to the interaction between shock wave and boundary layer.

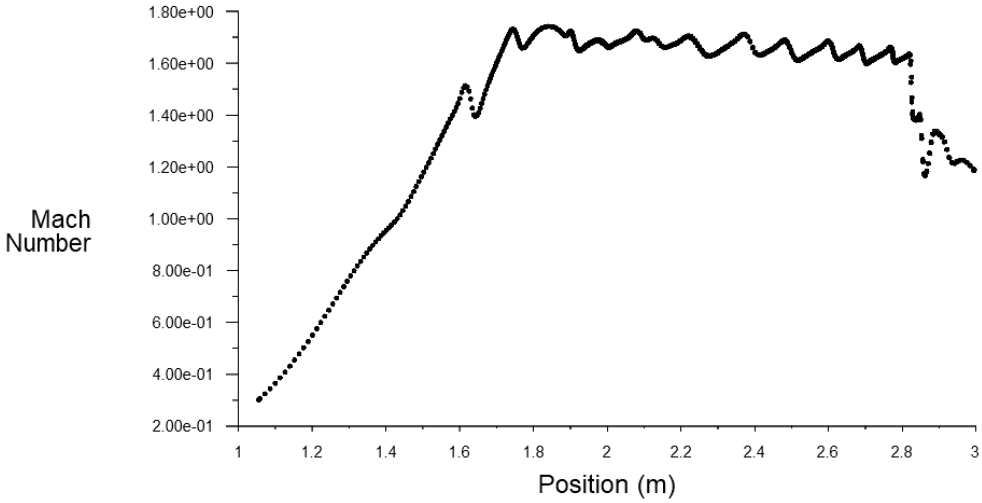

Figure 8. Mach number along the middle of the nozzle section from the divergent and curved section.

Fig. 8 shows the Mach number variation along the middle of the nozzle section from upstream to downstream. In the graph, we noticed that the Mach number varies between approximately 1.8 and 1.6 which is associated with the sequence of oblique shocks along the curved part of the nozzle as shown in Fig. 7a and 7b. For this analysis case, only the case without the collector was considered.

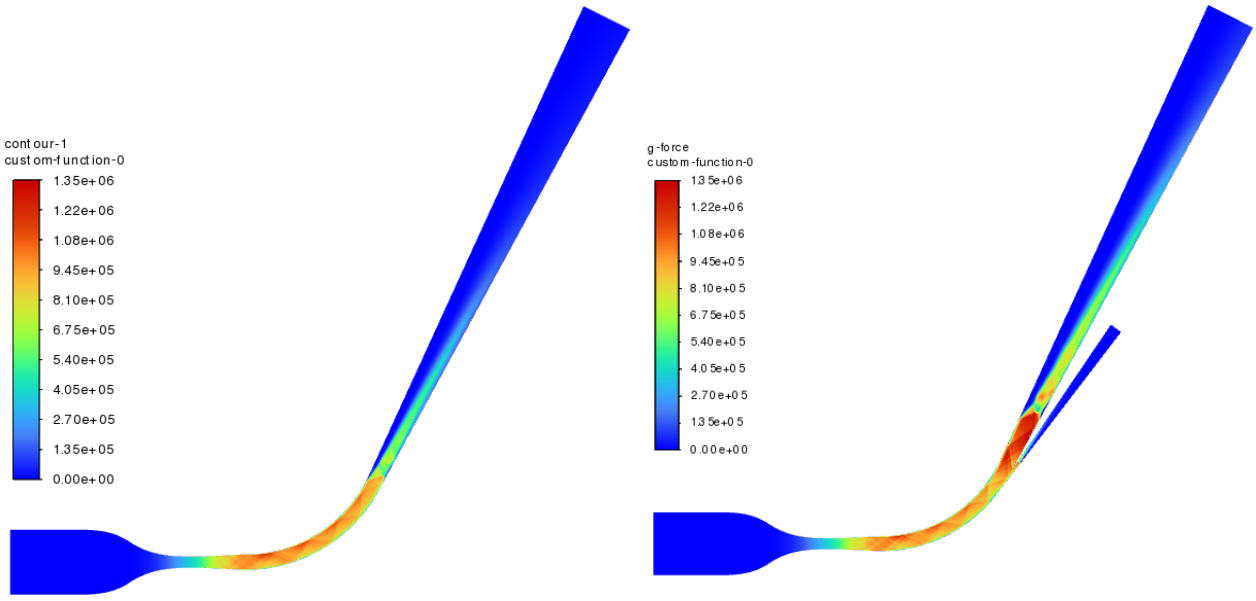

Figures 9a and 9b. The G Force distribution for the case without the gas collector (left) and with the gas collector (right). A G force centrifugal acceleration of up to approximately 118000 G and 135000 G on the smaller radius side and of approximately 95000 G on the larger radius part is observed in both figures. As in Figure 8, the oblique shocks that are reflected.

As observed in Fig 9a., the G force target estimated for 100000 G resulted in the range from 94800 to 118000 between the throat of the nozzle and the inlet of diffuser. The Mach number along the middle of the nozzle denoted by figure 8 indicates a mean value of 1.70 with a standard deviation of +/- 0.10 in the supersonic region. In Fig. 9b, the target is estimated 110000 G, with the range between 95000 and 135000 and a Mach number varying between 1.59 and 1.82.

On the collector, an oblique shock wave occurs internally in the innermost position on the upper wall, being the same close to the bottom of the main nozzle. The settlement of the velocity and pressure field is carried out with 75% of the collector length.

In the same analysis to obtain initial velocity ranges using the supersonic straight section, with the same inlet, outlet pressure and NPR in the curved nozzle case, the value range is according to the supersonic section of the straight case. Only in regions of the lower radius arc whose Mach number has reached higher numbers, such as regions in red of figure 8 demonstrate, according to equation (2). The increase in the Mach number is due to the radial acceleration component that the gas is subjected to in the flow, denounced by the G force.

The difference in Mach values has a cause in the effects of centrifugation, where the gas is pushed to the outside of the nozzle, so the inner part (with a lower radius) the gas becomes more rarefied, so an expansion occurs and gas has its Mach number increased in that region; on the other hand, in the external region of the curve with larger radius, the gas is more compressed due to centrifugation, so the Mach number decreases.

After the main shock region, as the gas expands more in the inner part with lower radius when it arrives at the diffuser inlet, the Mach is larger on that side, side with lower radius, and the Mach is smaller on the part with larger radius, so the main normal shock will come out slanted.

On the other hand, the convergence process for the treatment of residuals was more challenging, with a greater number of iterations in respect to the straight case.

Besides the configuration with a radius of 0.2214 m and arc angle of 63.42 (Fig. 4), named as case I (without the gas collector) presented above and V (with the gas collector), in order to increase the centrifugal force, three additional configurations were considered, named as case II, III and IV without the gas collector. For these three cases, the arc angle was increased to 90 and 120 degrees and the curvature radius decreased to 0.1561 m, the combined values are shown in Table 3. The numerical simulation of these three cases were carried out with a lower outlet pressure in order to guarantee the shock waves to occur at the diffusor inlet (that is, to keep supersonic flow inside the main duct downstream the diffusor). The range of outlet pressures that would satisfy this condition is around 40 to 45 kPa using the same mesh sizes and general distribution as described above (shown in Figs. 5.1 to 5.3) with the turbulence model k-ε RNG.

For all cases, the convergence criteria were reached according to section 4.2. With these additional cases with respect to case I, the convergence criteria were more difficult to be achieved due to the unconventionality of the geometry and the boundary conditions, requiring an increase in iterations, reaching the range between 8000 and 10000 to reach the criteria.

The cases with the gas collector identified as cases V and VI are described in Table 3. The turbulence model used for the simulation of case V as presented before is the k-ε RNG. Finally, in order to compare the numerical results with a different turbulence model, an additional case, identified as case VI, was proposed with the turbulence model k-ω SST.

Table 3. Cases with different configurations

Case	Gas collector present	Turbulence Model	Radius (m)	Arc angle (°)	Maximum Mach Number	Maximum G-force	Outlet Pressure (kPa)
I	No	k-ε RNG	0.2214	63.42	1.98	118000	65000
II	No	k-ε RNG	0.2214	90.00	2.38	144000	45000
III	No	k-ε RNG	0.1561	90.00	2.43	206000	40000
IV	No	k-ε RNG	0.1561	120.00	2.50	214000	40000
V	Yes	k-ε RNG	0.2214	63.42	2.27	135000	45000*
VI	Yes	k-ω SST	0.2214	63.42	2.38	146000	45000*

*diffuser and collector outlet pressure

With the decrease in the radius and the increase in the arc angle, as predicted, there was an increase in the G force and the local Mach Number for each simulated case, in addition to need to reduce the outlet pressure.

In cases V and VI, due to the presence of the gas collector in comparison with the previous cases, 45000 kPa of outlet pressure was required to keep the shock wave at the diffuser inlet, same as case II. By comparing the numerical results of cases V and VI. in terms of the use of the turbulence models, respectively k-ε RNG and k-ω SST, the Mach number and G force field did not show significant difference. Quantitatively, a decrease of 4.84% for the maximum Mach number and an increase of 5.65% for the maximum G-force were respectively obtained with the values shown in Table 3.

5. CONCLUSION

The numerical results were achieved in which the physical conditions were imposed for the proposed flow. Noticeably, as shown in Fig. 9a and 9b, the numerical results show that at the diffuser inlet region the main shock wave is deflected as an effect of the nozzle curvature. In addition, in Fig. 9a and 9b, along the supersonic flow region, due to the nozzle curvature, a series of weak shock waves that reflects at the nozzle wall are also noticed. With the boundary conditions in relation to pressure and temperature setups present in Table 1, the supersonic conditions for the flow were

obtained. Simulations results showed that centrifugal acceleration increased G-force number and arc angle with decreasing radius for the six tested cases described in Table 3.

By decreasing the radius, however, to ensure the physical conditions of the normal shock at the diffuser inlet, the outlet pressure was adjusted from 65000 to 45000 and 40000 Pa. With the introduction of the collector, there was a marginal refinement in the mesh as a whole. The simulation results for each of the two turbulence models considered (k-ε RNG and k-ω SST) presented quite similar behavior, as such as an example of reference, the maximum Mach number difference was 0.11 (4.84%) and G-force difference was 11000 (5.65%) as presented in Table 3.

For future simulations, the desired targets are in the range of 270000 G and 800000 G according to (Duan et al., 2019 and Wen et al. 2010) as the recommended G-force level to achieve an appropriate gas separation; as such the geometry should be altered in conjunction with the boundary conditions. In addition, the use of the gas considered with a real gas law behavior (instead of ideal gas) should also be considered for the simulations. Finally, the gas with two components mixed, such as methane and CO_2, including condensation effects of CO_2, should also be taken into account for future numerical investigations.

6. ACKNOWLEDGMENTS

I would like to thank the RCGI (Research Center for Greenhouse Gas Innovation) and Shell for their support and promotion of the project, as well as the Polytechnic School of University of São Paulo and Federal University of ABC.

7. REFERENCES

Ansys Inc (2013), “FLUENT USER’S GUIDE”.< https://www.ansys.com/>.

Barth, T.J., Jespersen, D.C., 1989. *The design and application of upwind schemes on unstructured meshes*, AIAA PAPER 89-0366.

Berger, A. H., Wang, Y., Bhown, A. S., Castrogiovanni, A., Kielb, R., & Balepin, V. (2017). *Thermodynamic Analysis of Post-combustion Inertial CO_2 Extraction System.* In *Energy Procedia* (Vol. 114, pp. 7–16). Elsevier Ltd.

Cao, X., Bian, J., *Supersonic separation technology for natural gas processing: A review, Chemical Engineering and Processing - Process Intensification*, Volume 136, 2019. ScienceDirect.

Duan, Z., Ma, Z., Guo, Y., Zhang, J., Sun, S., Liang, L. *Study on Supersonic Dehydration Efficiency of High Pressure Natural Gas (2019)*, College to Electromechanical Engineering, Qingdao University of Science and Technology.

Lima, P. C. R. 2016 “*Gás Natural: a sua utilização na geração de energia elétrica no Brasil*”. jan. 2020. < http:// www.desenvolvimentistas.com.br/blog/blog/2016/01/14/a-solucao-para-o-co2-do-pre-sal/>.

Maliska C., 2004. *Transferência de calor e mecânica dos fluidos computacional*. 2nd edition, LTC (in portuguese).

Versteeg, H. K. and Malalasekera,W. *An introduction to computational fluid dynamics - the finite volume method*. [S.l.]: Addison-Wesley-Longman, 2007.

Wen, C., Cao, X., Yang, Y., Zhang, Y., *Evaluation of natural gas dehydration in supersonic swirling separators applying the Discrete Particle Method*, Advanced Powder Technology, Volume 23, Issue 2, 2012,

Wen, C., Cao, X., Zhang, J., & Wu, L. *Three-dimensional Numerical Simulation of the Supersonic Swirling Separator*. International Society of Offshore and Polar Engineers. 2010.

Yang, Y.; Wen, C.; Wang, S.; Feng, Y. *Numerical simulation of real gas flows in natural gas supersonic separation processing*, Journal of Natural Gas Science and Engineering. 2014.

8. RESPONSIBILITY NOTICE

The authors are the only responsible for the printed material included in this paper.